Journal of Materials Chemistry A

Accepted Manuscript

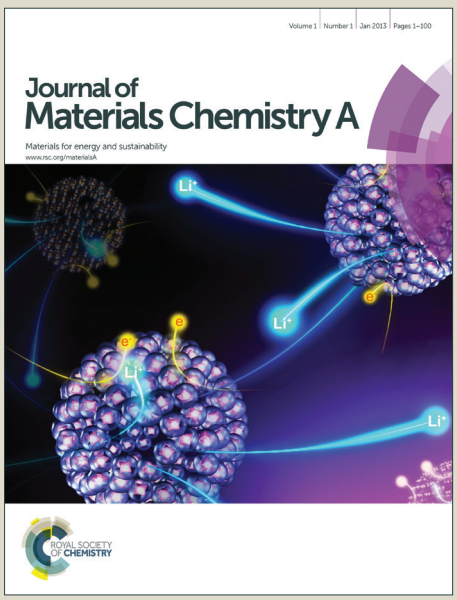

ROYAL SOCIETY OF CHEMISTRY

www.rsc.org/materialsA

Electro-codeposition of Vanadium Oxide-Polyaniline Composite Nanowire Electrodes for High Energy Density Supercapacitors

Ming-Hua Bai‡[a], Tian-Yu Liu‡[b], Feng Luan[a,b], Yat Li[b] and Xiao-Xia Liu*[a]*

[a] Department of Chemistry, Northeastern University, Shenyang, 110819, China.

[b] Department of Chemistry and Biochemistry, University of California, Santa Cruz, CA, 95064, USA.

‡ These authors contributed equally to this work.

* Corresponding authors' Emails: xxliu@mail.neu.edu.cn and yli@chemistry.ucsc.edu

Abstract

To meet the increasing demand for high energy density supercapacitors, it is crucial to develop positive and negative electrodes with comparable energy density. Previous studies have primarily focused on the development of positive electrodes, while negative electrode is relatively less explored. Here we report an electro-codeposition method to synthesize a high performance negative electrode composed of vanadium oxide (V_2O_5) and polyaniline (PANI) composite. Scanning electron microscopy revealed that the composite film is composed of one-dimensional polymer chain. Energy-dispersive X-ray spectroscopy (EDX) and X-ray diffraction (XRD) confirmed successful incorporation of V_2O_5 into PANI chains. Significantly, the V_2O_5/PANI composite nanowires exhibited a wide potential window of 1.6 V (between −0.9 and 0.7 V *vs.* SCE) and a maximum specific capacitance of 443 F/g (664.5 mF/cm^2). The flexible symmetric supercapacitor assembled with this composite film yielded a maximum energy density of 69.2 Wh/kg at the power density of 720 W/kg, and a maximum power density of 7200 W/kg at the energy density of 33.0 Wh/kg. These values are substantially higher than those of other pure V_2O_5 or PANI based supercapacitors. Moreover, the assembled symmetric supercapacitor device showed an excellent stability with 92 % capacitance retention after 5000 cycles. The capability of synthesizing high performance composite electrodes using electro-codeposition method could open up new opportunities for high energy density supercapacitors.

Keywords: vanadium oxide, polyaniline, electro-codeposition, symmetric supercapacitors

Introduction

Development of high performance supercapacitors is highly desirable to meet the increasing demand for energy storage devices. [1-3] Carbon materials have been extensively employed as electrodes for supercapacitors. However, their relatively low specific capacitance (~90-250 F/g) and low energy density are major drawbacks for practical applications.[4-7] Pseudo-capacitive materials, including transition metal oxides and conducting polymers are promising candidates for supercapacitor electrodes since they have much higher capacitance compare with carbon based materials. [5, 8] But the energy density of these materials is usually limited by their narrow potential windows in aqueous electrolytes, in most cases less than 1 V. According to the equation of calculating energy density (E) for supercapacitors, $E = \frac{1}{2}CV^2$, where C is specific capacitance and V is operational voltage, there are two approaches to boost the energy density of supercapacitors. First, it is important to increase specific capacitance by replacing conventional carbon based electrode with pseudo-capacitive electrodes. Second, it is crucial to expand the operational voltage of the supercapacitor device. [9, 10] Previous studies have been primarily focused on fabricating high energy density pseudocapacitive positive electrodes. [4, 11] To achieve high energy density supercapacitors, a negative electrode with comparable energy density to cathode is essential. However, the development of anode is less explored.

Some transitional metal oxides, such as indium oxide, vanadium oxide and tungsten oxide are pseudo-capacitive materials with a potential window extended to negative potential and thus can be used as alternatives to carbon based electrode. Among them, vanadium oxide has attracted a lot of attention. [12] Its layered structure allows efficient ions diffusion. And it is

anticipated that vanadium oxide can achieve high pseudocapacitance due to the presence of multiple stable oxidation states of vanadium. [13] For example, it has been reported that electro-spun V_2O_5 nanofibers exhibited good stability in the potential range between -1 and 0 V *vs.* SCE. [14] In addition, V_2O_5-polypyrrole core-shell nanocomposite electrode achieved a high specific capacitance of 308 F/g (at a current density of 0.1 A/g) in a wide potential window of 1.0 V (between -0.9 and +0.1 V *vs.* SCE). [15] Therefore, V_2O_5 is a good candidate for negative electrode material.

Polyaniline (PANI) has been widely studied as a positive electrode material due to its ease of synthesis and high capacitance (max. value: 3407 F/g) [16]. Moreover, PANI has high hydrogen evolution overpotential and large operational potential in positive potential. Therefore, PANI is a suitable material to combine with those transition metal oxides that have a negative potential window to form asymmetric supercapacitors. [17-19] In this work, we demonstrated an electro-codeposition method to synthesize V_2O_5-PANI composite nanowires (NWs) on carbon cloth. The composite electrode exhibited an exceptionally large potential window of 1.6 V from -0.9 to +0.7 V *vs.* SCE. Significantly, a flexible symmetric supercapacitor assembled with the composite nanowire electrode achieved an excellent energy density of 69.2 Wh/kg.

Experiment

Materials

Aniline was distilled prior to use. All other chemicals were analytical grade and used as received. A piece of carbon cloth (~1 cm^2, SGL group, German) was used as counter electrode and a saturated calomel electrode (SCE) was used as reference electrode. The

carbon cloth with geometric area of 1 cm^2 was used as the working electrode for electro-codeposition.

Preparation of V_2O_5, PANI and V_2O_5-PANI composite NWs on carbon cloth

Carbon cloth was scanned in 2.0 M H_2SO_4 aqueous solution at 100 mV s^{-1} within −1.2~1.6 V *vs.* SCE to remove surface contamination prior to electro-codeposition. V_2O_5-PANI (VP) composite NWs VP-0.5, VP-1, VP-2, VP-3, VP-4, and VP-5 were electrochemically deposited on carbon cloth by 40 scans between −0.2 and 0.9 V at a scan rate of 20 mV/s in 0.1 M aniline aqueous solution containing 0.05, 0.1, 0.2, 0.3, 0.4 and 0.5 M vanadyl sulfate ($VOSO_4$), respectively. The pH value of solutions for electro-codeposition was adjusted to 1.8 using concentrated H_2SO_4. For comparison, V_2O_5 and PANI NWs were respectively prepared in 0.1 M $VOSO_4$ and 0.1 M aniline solutions, under the same conditions as VP nanowires. The electrodes were washed thoroughly with distilled water and dried in vacuum at 50 °C for 24 h. The loading mass of V_2O_5, PANI and VP-1 film were measured to be 0.80, 1.02 and 1.50 mg/cm^2 respectively.

Fabrication of flexible VP-1 symmetric supercapacitors

Symmetric supercapacitors were assembled by assembling two pieces of VP-1 composite electrodes together, using a piece of filter paper (Xinhua Corporation, China) as separator. LiCl/PVA gel was used as electrolyte. LiCl/PVA was prepared as follows: 3 g PVA was mixed with 30 mL 5 M LiCl aqueous solution and heated at 85 ^oC under vigorous stirring until a clear gel was formed. Electrodes and separator were soaked in the LiCl/PVA gel electrolyte for 5 minutes and solidified at room temperature for 6 h. They were assembled together and kept at 45 °C for 12 h to remove excess water in the electrolyte. After heating,

the entire device was wrapped with polyimide tape and sealed with epoxy resin to avoid absorbing moisture from air. The working area of the supercapacitor was 1 cm^2 and total mass loading of two electrodes was 1.98 mg/cm^2.

Material characterization

The composition of samples was investigated by X-ray diffraction (XRD, D8 Advance, Bruker, Germany) and Fourier transform infrared spectroscopy (FT-IR, A Spectrum One, Perkin-Elmer, USA). Morphologies were characterized by scanning electron microscope and energy-dispersive X-ray spectroscopy (SEM and EDX, LEO SUPRA 35, Carl Zeiss, Germany). Electrochemical performance was evaluated in a traditional three-electrode electrolytic cell by cyclic voltammetry (CV) at various scan rates and galvanostatic charge-discharge experiment in 5.0 M LiCl between −0.9 and 0.7 V *vs.* SCE at various current densities. Electrochemical impedance spectroscopy (EIS) measurements were conducted in a frequency range of 100 mHz to 40 kHz in 5 M LiCl at open circuit potential with a perturbation of 5 mV. All electrochemical experiments were conducted using VMP3 multi-channel electrochemical analyzer system (Bio-Logic-Science Instruments, France). Mass loading was measured by Sartorius BT25s semi-micro balance with an accuracy of 0.01 mg.

Results and discussion

VP-1, PANI, V_2O_5 and bare carbon cloth were characterized by XRD. As shown in Fig 1a, both VP-1 and V_2O_5 exhibit signals centered at 22° and 51°, which corresponding to characteristic diffraction peaks of V_2O_5 crystalline planes of (1 0 1) and (0 2 0) (JSPDS card

No. 41-1426). [14, 20] Characteristic diffraction peak of V_2O_5•$3H_2O$ (JSPDS card No. 07-0332) at 28° also appears on the XRD spectra of VP-1 and V_2O_5. PANI did not show any peaks due to its amorphous nature. Fig. 1b shows the Fourier transform-Infrared spectra of VP-1 and PANI. Both VP-1 and PANI spectra exhibit main characteristic bands of PANI. The stretch vibration band of benzenoid rings locates at 1494 cm^{-1}, which is blue shifted compared to that of PANI (1476 cm^{-1}). Stretching band of the quinoid rings overlaps with the 1638 cm^{-1} band of the in-plane bending mode from structural water.[18, 21] Band appears at 1303 cm^{-1} can be attributed to C–N stretch of secondary aromatic amine of PANI chain. The characteristic band of protonated PANI in VP-1 appears at 1129 cm^{-1}, which is also blue shifted compare to that of PANI spectrum (1103 cm^{-1}). The blue-shift of some bands indicates a synergistic effect of electro-codeposition. [18] The V=O vibration band appears at 973 cm^{-1} for VP-1, which is red shift compared with original place (~990 cm^{-1}). [22] It suggests that some coordinated water molecules' positions are occupied by the inserted polymer. [22] Band at 745 cm^{-1} can be attributed to the V-O stretching vibration. [22, 23] These results prove that the VP-1 composite film composes of both V_2O_5 and PANI materials.

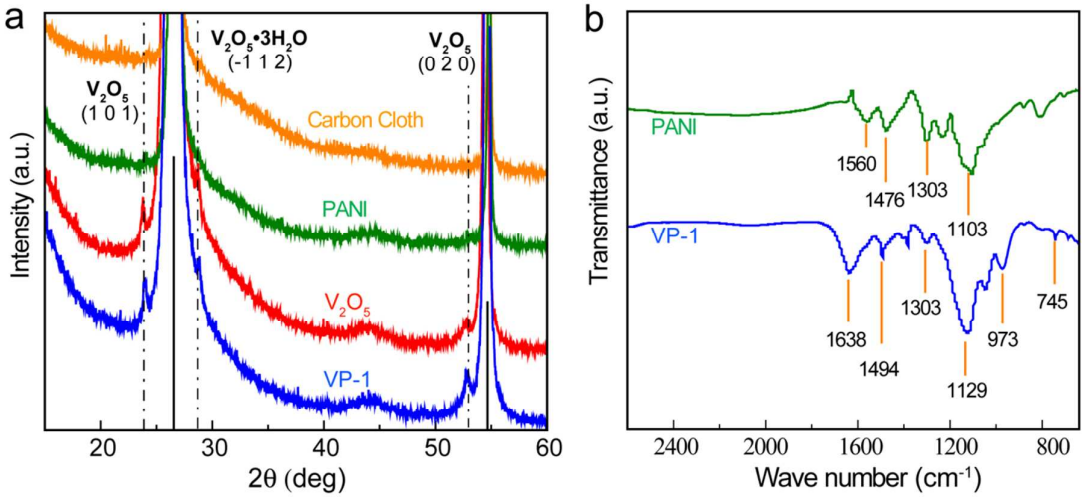

Figure 1. (a) XRD spectra collected for VP-1, V_2O_5 and PANI deposited on carbon cloth. Dashed lines highlight the characteristic diffraction peaks of V_2O_5 and $V_2O_5 \cdot 3H_2O$. Solid lines highlight the diffraction peaks of carbon cloth substrate. (b) FT-IR spectra of PANI and VP-1.

The morphologies of PANI, V_2O_5 and VP-1 samples were investigated by SEM (Fig. 2). Pure V_2O_5 forms large particles (Fig. 2b). The VP-1 was directed to grow in one dimensional (1D) direction to form nanofibers upon electro-codeposition (Fig 2c). 1D nanofiber is the intrinsic morphology of PANI. [24] However, this structure is hard to obtain due to secondary growth deriving from the presence of excessive amount of aniline monomers, which leads to irregular morphology due to agglomerated polymer chains (Fig.2a). [24] Numerous methods have been reported to suppress this secondary growth including aqueous/organic interfacial polymerization, rapidly-mixed reaction, ultrasonic irradiation, dilute polymerization, *etc.* to synthesize 1-D PANI structure. [24-27] In this situation, when VO^{2+} appears in the electro-codeposition bath, the deposition of V_2O_5 from VO^{2+} ($2VO^{2+}+3H_2O \rightarrow V_2O_5+6H^{+}+2e^{-}$) [28] will consume part of the anodic positive charges, which are the reactant for aniline polymerization, and thus lowering the concentration of reactant and favoring formation of 1D polymer chain. In addition, the incorporation of V_2O_5 would be helpful to effectively avoid the entanglement of PANI chains, which is observed similarly in PANI/mesoporous carbon-SiO_2 [29] and PANI/MnO_2 [19] composites.

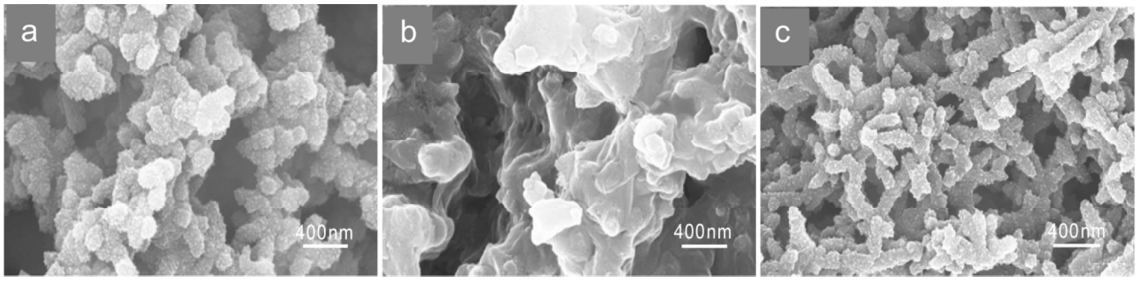

Figure 2. SEM images of (a) PANI, (b) V_2O_5, and (c) VP-1 deposited on carbon cloth substrate.

To study the electrochemical performance of the VP-1 composite, cyclic voltammetry and galvanostatic charge-discharge experiment were conducted in 5 M LiCl aqueous electrolyte. The cyclic voltammogram (CV) of VP-1 together with those of PANI and V_2O_5 are shown in Fig. 3a. The CV of PANI shows a typical redox pairs: B/B' at 0.16/-0.10 V *vs.* SCE corresponding to the transition between leucoemeraldine and emeraldine states of PANI, C/C' at 0.58/0.40 V *vs.* SCE corresponding to exchange between emeraldine and pernigraniline states. [17, 18] The peaks A and D of V_2O_5 are related to Li^+ de-intercalation and peaks A' and D' are corresponded to Li^+ intercalation. [30, 31] The CV curve of VP-1 shows a combined shape of PANI and V_2O_5, and also has the largest capacitance. The results again prove the successfully incorporation of V_2O_5 into PANI. The high capacitance of VP-1 composite is due to the synergistic effect of V_2O_5 and PANI. More importantly, the VP-1 exhibited a wide potential window of 1.6 V. We did not observe oxygen and hydrogen evolution on the electrodes. The extension of working potential is believed to be due to the combination of the high hydrogen evolution potential offered by V_2O_5 under negative polarization together with high oxygen overpotential when PANI is used as positive electrode. [14, 32]

To further evaluate the capacitance of VP-1 NWs, the galvanostatic charge-discharge

experiment was conducted from -0.9 V to 0.7 V *vs.* SCE at 0.5 mA/cm^2 in 5 M LiCl aqueous electrolyte (Fig.3b). The discharge time of VP-1 is much longer that those of PANI and V_2O_5, indicating the higher charge storage capacity of VP-1 electrode. The capacitance of VP-1 is calculated to be 443 F/g according to the equation $C_m=I\times t/(\Delta U\times m)$, where C_m (F/g) is the specific capacitance, I and Δt are the charge/discharge current (A) and time (s), ΔU is the potential window (V), and m is the mass loading of film (g). This value is substantially higher than those obtained for V_2O_5 electrode (217 F/g) and PANI electrode (241 F/g), in consistent with CV analysis. Fig. 3c summarizes the specific capacitance of VP-1, PANI and V_2O_5 under different charge-discharge current densities. It shows that VP-1 sample has higher capacitance than PANI and V_2O_5 at all current densities. Moreover, the VP-1 electrode showed excellent rate capability, which is even comparable to some double layer based supercapacitors. [33, 34] When the charge current increased from 0.5 to 5 mA/cm^2, the gravimetric capacitance of VP-1 still maintained as high as 281 F/g. Galvanostatic charge-discharge experiment was carried out at a current density of 5 mA/cm^2 in 5 M LiCl aqueous electrolyte to further evaluate the stability of those electrodes. As shown in Fig. 3d, V_2O_5 and PANI only retain 49% and 63% of its initial capacitance after 1000 cycles, respectively. In contrast, VP-1 exhibited much better cycling stability with capacitance retention of 87% after 1000 cycles under the same conditions. These results suggested VP-1 is an excellent pseudo-capacitive electrode material.

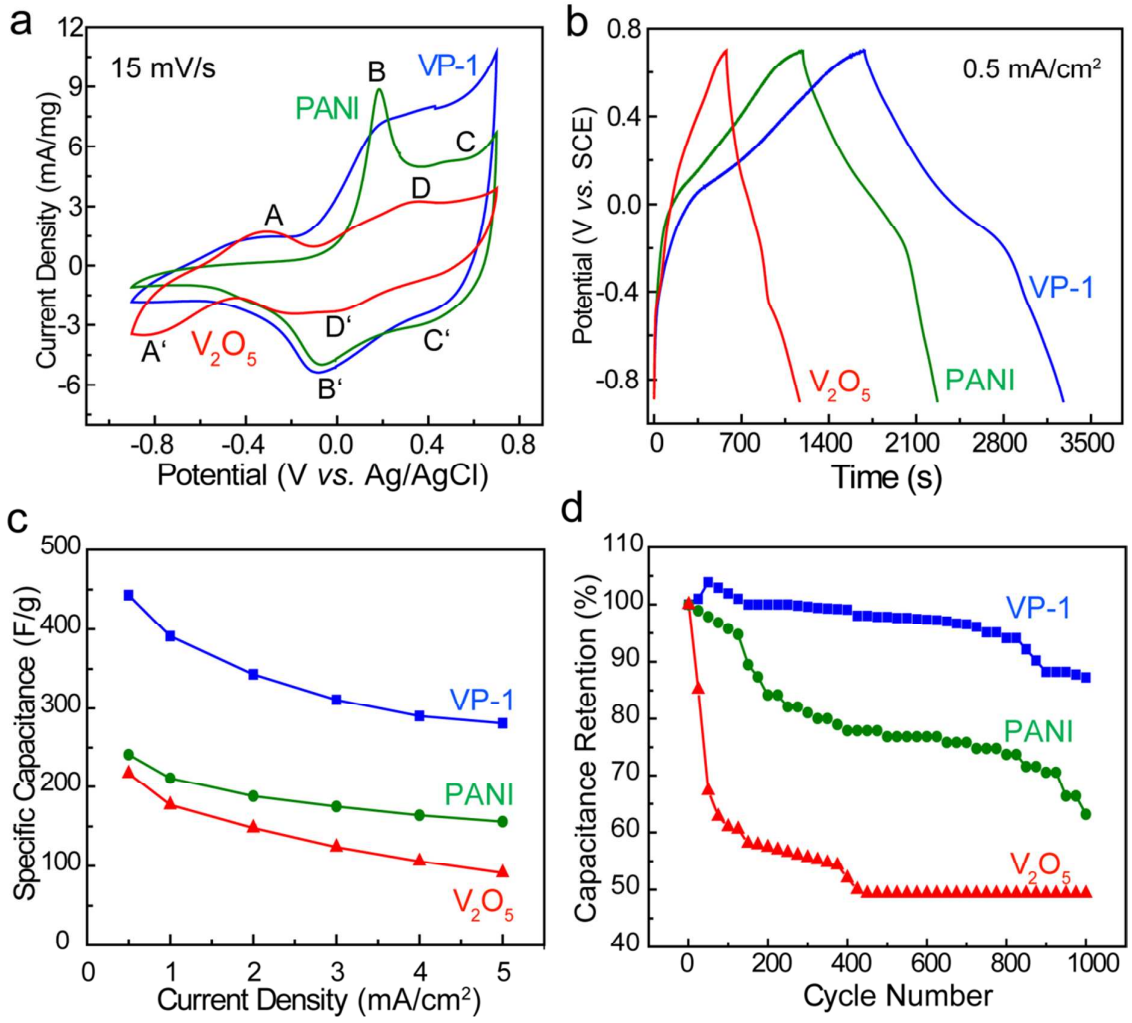

Figure 3. Electrochemical performance of VP-1, PANI and V_2O_5 collected in 5 M LiCl solution. (a) CV curves collected at a scan rate of 15 mV/s; (b) galvanostatic charge-discharge curves collected at a current density of 0.5 mA/cm^2; (c) rate-capabilities and (d) cycling stability measured by galvanostatic charge-discharge experiment at a current density of 5 mA/cm^2.

To further optimize the performance of V_2O_5-PANI composite, we investigated the interplay between the ratio of V_2O_5 to PANI and properties of VP composites. VP-0.5, VP-1, VP-2, VP-3, VP-4 and VP-5 were synthesized from 0.1 M aniline solutions containing 0.05, 0.1, 0.2, 0.3, 0.4 and 0.5 M $VOSO_4$, respectively. To determine the amount ratio of V_2O_5 to

PANI in obtained VP films, energy-dispersive X-ray spectra (EDX) of those six composites were collected (Fig. 4a). In the EDX spectra, V signal originated from V_2O_5, while S signal came from SO_4^{2-} ions doped in the PANI backbone. Assuming all six PANI samples have similar doping concentration, the amount of SO_4^{2-} should be directly proportional to the amount of PANI. Thus, the V/S peak intensity ratio represents the amount ratio between V_2O_5 and PANI. As shown in Fig. 4b, the V/S ratio increase with the increase of $VOSO_4$ concentration in electro-deposition solution. To further evaluate the electrochemical performance, galvanostatic charge-discharge experiment was conducted. Fig. 4c shows the galvanostatic charge-discharge curves of VP-0.5, VP-1, VP-2, VP-3, VP-4 and VP-5 collected at a current density of 2 A/g. The VP-1 sample has the longest discharge time, exhibiting the largest gravimetric capacitance (Fig. 4d). EIS measurements were carried out for all VP samples. Nyquist plots in the low-frequency domain show that the VP-1 composite film exhibits a slope closer to 90^o than others, indicating that VP-1 has the best capacitive behavior and the lowest diffusion resistance for ions. [35, 36] Moreover, VP-1 possessed the lowest combined series resistance (R_s) obtained from crossing of the high-frequency domain end and the real component axis (Fig. 4f), [37] suggesting it has improved electrical conductivity and fast ion transport. The EIS data explain the superior performance of VP-1 over the other VP samples.

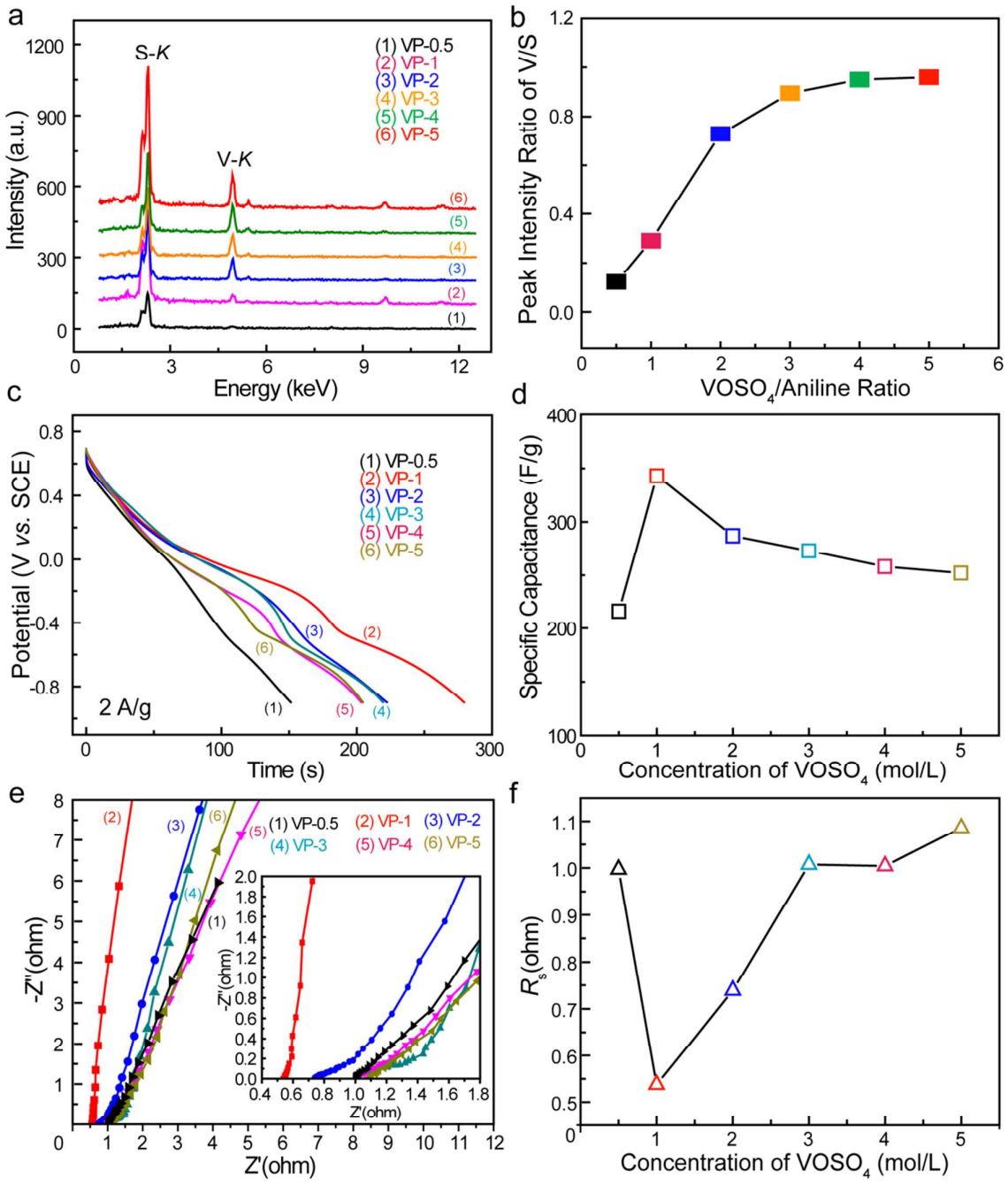

Figure 4. (a) EDX spectra of VP composite films; (b) peak intensity ratio of V/S from VP films electro-deposited in solutions containing different $VOSO_4$ concentration; (c) galvanostatic charge-discharge curves at a current density of 2 A/g in the range of -0.9 V~ 0.7 V *vs.* SCE in 5 M LiCl aqueous solution; (d) plots of specific capacitance against concentration of $VOSO_4$; (e) Nyquist plots of VP composite films collected in a frequency

range from 100 mHz to 40 kHz in 5 M LiCl at open circuit potential with a perturbation of 5 mV. Inset shows the high-frequency domain of the Nyquist plots; (f) combined series resistance against concentration of $VOSO_4$.

To understand the trend of specific capacitance changed with $VOSO_4$ concentration, SEM was conducted to investigate morphologies of VP-0.5, VP-1, VP-2, VP-3, VP-4 and VP-5 (Fig. 5). In Fig.5a and 5b, VP-0.5 and VP-1 have similar nanorod morphology. The larger specific capacitance of VP-1 compared with VP-0.5 was believed to be the increase amount of V_2O_5 incorporated. However, when the concentration of $VOSO_4$ was further increased, nanorods started to aggregate with each other and caused a reduction of effective surface area. It explains the decrease of specific capacitance as the amount of V_2O_5 increased.

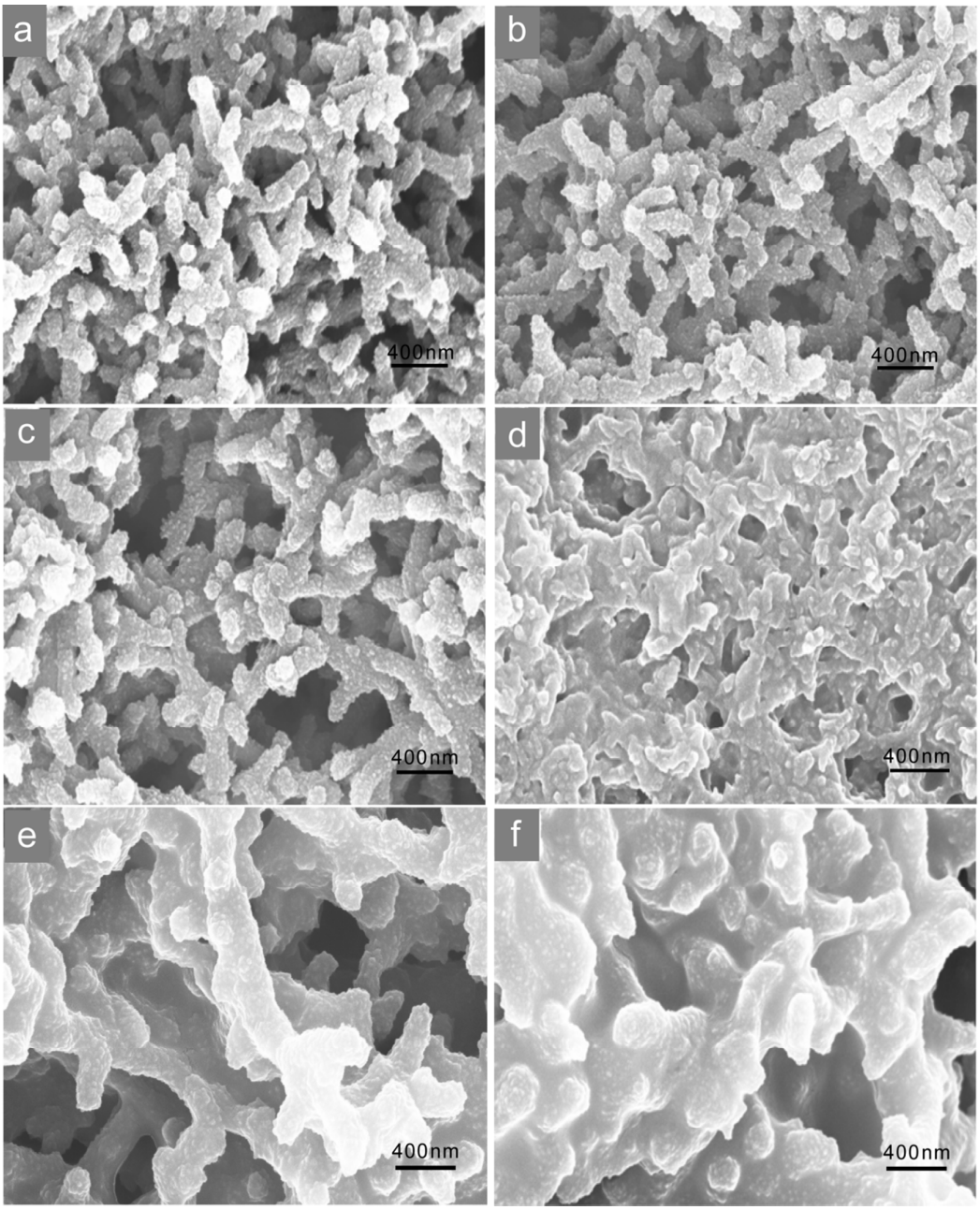

Figure 5. SEM images of (a) VP-0.5, (b) VP-1, (c) VP-2, (d) VP-3, (e) VP-4 and (f) VP-5 composite films.

To evaluate the performance of the VP-1 composite electrode for application as flexible supercapacitor devices, symmetric supercapacitors (SSCs) were fabricated by assembling two identical pieces of VP-1 electrodes together with a piece of filter paper as separator and LiCl/PVA as electrolyte. The SSC device is denoted as VP-1//VP-1. CV

measurements and galvanostatic charge-discharge experiments were conducted for VP-1//VP-1 SSC at various scan rates and current densities in an operational voltage between 0 and 1.6V. The device exhibited CV curve without obvious distortion even at a scan rate of 100 mV/s (Fig. 6a), indicating fast charge-discharge property of the device is good. Additionally, charge-discharge curves (Fig. 6b) show nearly symmetric triangle shape with some plateaus, confirming its pseudo-capacitive behavior and good reversibility within the 1.6 V voltage window. Long-term stability is another concern of the applications of supercapacitors. Fig. 6c shows the stability of the VP-1//VP-1 collected at a current density of 5 mA/cm^2 for 5000 cycles. Significantly, the VP-1//VP-1 SSC exhibited an excellent cycling stability with 92% capacitance retention after 5000 cycles. This value was also better than the values reported for other asymmetric supercapacitors using inorganic oxide as negative electrode, such as WO_3//RuO_2 (72% after 200 cycles), [38] $Ru_{0.36}V_{0.64}O_2$//Ni (83.5% after 1500 cycles), [39] WO_3-MoO_3//PANI (~80% after 2000 cycles) [40] and V_2O_5//PANI (73% after 2000 cycles). [14] In addition, the assembled SSC is also highly flexible. The device exhibited similar electrochemical performance at different bend angles (Fig. 6d), indicating its potential to be used as flexible energy storage device.

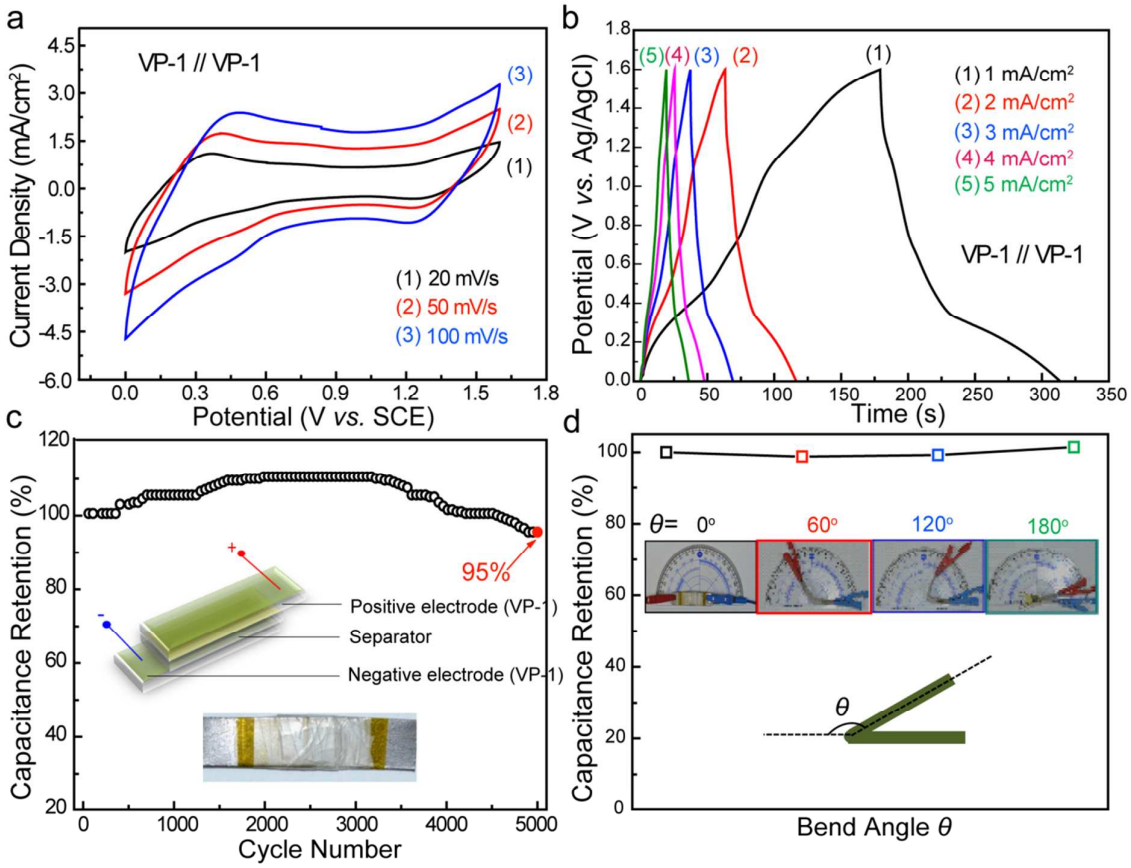

Figure 6. (a) CV curves and (b) galvanostatic charge-discharge curves collected for VP-1//VP-1 SSC at various scan rates and current densities. (c) Cycling stability of VP-1//VP-1 SSC collected by galvanostatic charge-discharge experiment at a current density of 5 mA/cm^2. Insets: schematic illustration and digital picture of the VP-1//VP-1 SSC. (d) Capacitance retention of the VP-1//VP-1 SSC device measured at different bend angles. Insets: schematic illustration of bend angle and pictures of the device under different bend conditions.

Furthermore, energy density and power density are also two important factors to evaluate the performance of supercapacitors. The energy density (E, Wh/kg) and power density (P, kW/kg) of VP-1//VP-1 SSC was calculated based on the equations $E=(0.5\times1000/3600)C\Delta U^2$ and $P=3600E/t$, respectively, where C is the specific capacitance (F/g) based on the active

materials on positive and negative electrodes, ΔU is the potential window (V) and t is the discharge time (s) measured by galvanostaic charge-discharge experiment. These results were summarized in Fig. 7. The VP-1//VP-1 achieved an excellent energy density of 69.2 Wh/kg at a power density of 0.72 kW/kg, and still maintain an energy density of 33.0 Wh/kg when the power density reached 7.2 kW/kg. These values are substantially higher than previously reported PANI based SSCs [41, 42] and even some asymmetric supercapacitors (ASCs) with comparable or larger potential window. [14, 18, 42-45] The high performance of the device can be attributed to the large pseudocapacitance as well as the wide potential window of the VP composite electrode.

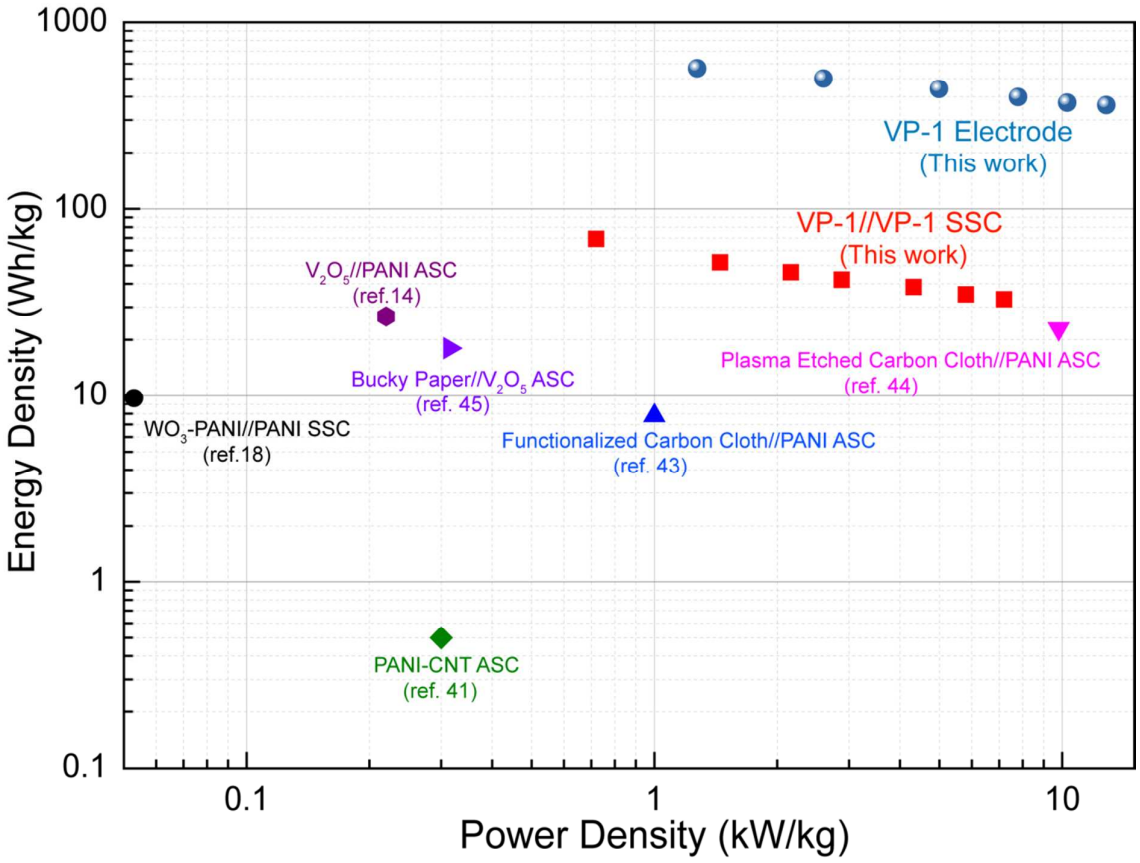

Figure 7. Ragone plots of VP-1//VP-1 flexible symmetric device and VP-1 single electrode measured in LiCl gel electrolyte. The values reported for other supercapacitor devices are

added for comparison.

Conclusions

In summary, we have demonstrated a facile electro-codeposition method to incorporate V_2O_5 in PANI matrix to synthesize VP composite films. The VP electrode displayed a wide charge storage potential window of 1.6 V and the highest capacitance of 443 F/g (664.5 mF/cm^2) at the current density of 0.5 mA/cm^2. The high performance of VP electrode is believed to be due to the formation of dense 1-D nanowires without aggregation. This unique nanostructure not only provides large surface area for ions absorption, but also facilitates electron transfer. Owing to its superior electrochemical performance of VP-1 film, the symmetric VP-1//VP-1 device obtains a maximum energy density of 69.2 Wh/kg at the current density of 0.5 mA/cm^2 and a maximum power density of 0.72 kW/kg at the current density of 5 mA/cm^2. These values are greatly enhanced compared to pure PANI or V_2O_5 based supercapacitors. The VP composite is a promising candidate for fabrication of high performance supercapacitors. .

Acknowledgement

Y.L. thanks the financial support of UCSC faculty startup fund. X.X.L. gratefully acknowledges supports of this work by National Natural Science Foundation of China (project number: 21273029) and Research Foundation for Doctoral Program of Higher Education of China (project number: 20120042110024).

References

1. Z. Fan, J. Yan, T. Wei, L. Zhi, G. Ning, T. Li and F. Wei, *Adv. Funct. Mater.*, 2011, **21**, 2366-2375.
2. X.-L. Wu, L.-Y. Jiang, F.-F. Cao, Y.-G. Guo and L.-J. Wan, *Adv. Mater.*, 2009, **21**, 2710-2714.
3. C. Peng, S. Zhang, X. Zhou and G. Z. Chen, *Energ. Environ. Sci.*, 2010, **3**, 1499-1502.

4. X. Lu, M. Yu, T. Zhai, G. Wang, S. Xie, T. Liu, C. Liang, Y. Tong and Y. Li, *Nano Lett.*, 2013, **13**, 2628-2633.
5. G. Wang, L. Zhang and J. Zhang, *Chem. Soc. Rev.*, 2012, **41**, 797-828.
6. G. Yu, L. Hu, M. Vosgueritchian, H. Wang, X. Xie, J. R. McDonough, X. Cui, Y. Cui and Z. Bao, *Nano Lett.*, 2011, **11**, 2905-2911.
7. J. Xiao and S. Yang, *RSC Adv.*, 2011, **1**, 588-595.
8. G. Wang, X. Lu, Y. Ling, T. Zhai, H. Wang, Y. Tong and Y. Li, *ACS Nano*, 2012, **11**, 10296-10302.
9. H. Yu, Q. Zhang, J. B. Joo, N. Li, G. D. Moon, S. Tao, L. Wang and Y. Yin, *J. Mater. A*, 2013, **1**, 12198-12205.
10. L. Y. Chen, J. L. Kang, Y. Hou, P. Liu, T. Fujita, A. Hirata and M. W. Chen, *J. Mater. A*, 2013, **1**, 9202-9207.
11. F. Wang, S. Xiao, Y. Hou, C. Hu, L. Liu and Y. Wu, *RSC Adv.*, 2013, **3**, 13059-13084.
12. C. Wu, F. Feng and Y. Xie, *Chem. Soc. Rev.*, 2013, **42**, 5157-5183.
13. J. Zhu, L. Cao, Y. Wu, Y. Gong, Z. Liu, H. E. Hoster, Y. Zhang, S. Zhang, S. Yang, Q. Yan, P. M. Ajayan and R. Vajtai, *Nano Lett.*, 2013, **13**, 5408-5413.
14. W. F. Mak, G. Wee, V. Aravindan, N. Gupta, S. G. Mhaisalkar and S. Madhavi, *J. Electrochem. Soc.*, 2012, **159**, A1481-A1488.
15. Q. Qu, Y. Zhu, X. Gao and Y. Wu, *Adv. Energy Mater.*, 2012, **2**, 950-955.
16. B. K. Kuila, B. Nandan, M. Böhme, A. Janke and M. Stamm, *Chem. Commun.*, 2009, 5749-5751.
17. X.-X. Liu, L.-J. Bian, L. Zhang and L.-J. Zhang, *J. Solid State Electrochem.*, 2007, **11**, 1279-1286.
18. B.-X. Zou, Y. Liang, X.-X. Liu, D. Diamond and K.-T. Lau, *J. Power Sources*, 2011, **196**, 4842-4848.
19. L. Chen, L.-J. Sun, F. Luan, Y. Liang, Y. Li and X.-X. Liu, *J. Power Sources*, 2010, **195**, 3742-3747.
20. E. Potiron, A. Le Gal La Salle, A. Verbaere, Y. Piffard and D. Guyomard, *Electrochim. Acta*, 1999, **45**, 197-214.
21. T. Hino, T. Namiki and N. Kuramoto, *Synthetic Met.*, 2006, **156**, 1327-1332.
22. F. Huguenin, E. A. Ticianelli and R. M. Torresi, *Electrochim. Acta*, 2002, **47**, 3179-3186.
23. C. G. Wu, D. C. DeGroot, H. O. Marcy, J. L. Schindler, C. R. Kannewurf, Y. J. Liu, W. Hirpo and M. G. Kanatzidis, *Chem. Mater.*, 1996, **8**, 1992-2004.

24. J. Huang and R. B. Kaner, *Chem. Commun.*, 2006, 367-376.
25. N. R. Chiou and A. J. Epstein, *Adv. Mater.*, 2005, **17**, 1679-1683.
26. J. Huang and R. B. Kaner, *Angew. Chem.-Int. Edit.*, 2004, **43**, 5817-5821.
27. X. Lu, H. Mao, D. Chao, W. Zhang and Y. Wei, *Macromol. Chem. Phys.*, 2006, **207**, 2142-2152.
28. A. Ghosh, E. J. Ra, M. Jin, H.-K. Jeong, T. H. Kim, C. Biswas and Y. H. Lee, *Adv. Funct. Mater.*, 2011, **21**, 2541-2547.
29. Y.-Q. Dou, Y. Zhai, H. Liu, Y. Xia, B. Tu, D. Zhao and X.-X. Liu, *J. Power Sources*, 2011, **196**, 1608-1614.
30. J. Światowska-Mrowiecka, V. Maurice, S. Zanna, L. Klein and P. Marcus, *Electrochim. Acta*, 2007, **52**, 5644-5653.
31. Y. Wang and G. Cao, *Electrochim. Acta*, 2006, **51**, 4865-4872.
32. V. Khomenko, E. Raymundo-Piñero and F. Béguin, *J. Power Sources*, 2006, **153**, 183-190.
33. S.-Y. Yang, K.-H. Chang, H.-W. Tien, Y.-F. Lee, S.-M. Li, Y.-S. Wang, J.-Y. Wang, C.-C. M. Ma and C.-C. Hu, *J. Mater. Chem.*, 2011, **21**, 2374-2380.
34. D. Liu, X. Wang, X. Wang, W. Tian, J. Liu, C. Zhi, D. He, Y. Bando and D. Golberg, *J. Mater. A*, 2013, **1**, 1952-1955.
35. Y. Song, J.-L. Xu and X.-X. Liu, *J. Power Sources*, 2014, **249**, 48-58.
36. X. Pan, Y. Zhao, G. Ren and Z. Fan, *Chem. Commun.*, 2013, **49**, 3943-3945.
37. M. Kim, Y. Hwang, K. Min and J. Kim, *Phys. Chem. Chem. Phys.*, 2013, **15**, 15602-15611.
38. K.-H. Chang, C.-C. Hu, C.-M. Huang, Y.-L. Liu and C.-I. Chang, *J. Power Sources*, 2011, **196**, 2387-2392.
39. C.-Z. Yuan, B. Gao and X.-G. Zhang, *J. Power Sources*, 2007, **173**, 606-612.
40. X. Xiao, T. Ding, L. Yuan, Y. Shen, Q. Zhong, X. Zhang, Y. Cao, B. Hu, T. Zhai, L. Gong, J. Chen, Y. Tong, J. Zhou and Z. L. Wang, *Adv. Energy Mater.*, 2012, **2**, 1328-1332.
41. Q. Liu, M. H. Nayfeh and S.-T. Yau, *J. Power Sources*, 2010, **195**, 7480-7483.
42. Jaidev, R. I. Jafri, A. K. Mishra and S. Ramaprabhu, *J. Mater. Chem.*, 2011, **21**, 17601-17605.
43. L.-J. Bian, F. Luan, S.-S. Liu and X.-X. Liu, *Electrochim. Acta*, 2012, **64**, 17-22.
44. P. Yu, Y. Li, X. Yu, X. Zhao, L. Wu and Q. Zhang, *Langmuir*, 2013, **29**, 12051-12058.
45. V. Aravindan, Y. L. Cheah, W. F. Mak, G. Wee, B. V. R. Chowdari and S. Madhavi, *ChemPlusChem*, 2012, **77**, 570-575.

ToC Entry

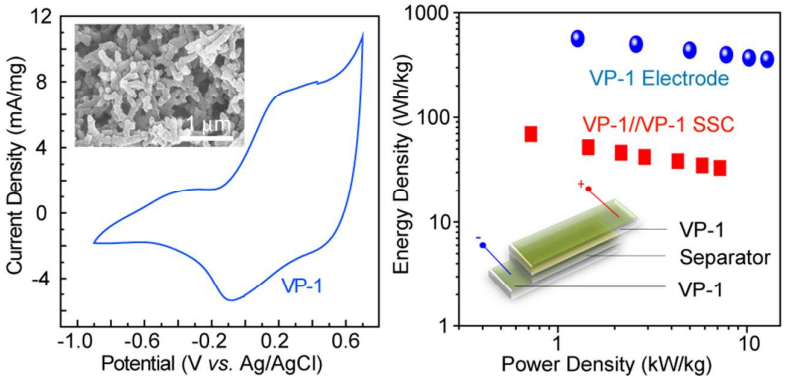

This work reports a flexible supercapacitor based on vanadium oxide-polyaniline composite (VP-1) with large potential window and high energy density.